# Anisotropy of $Ti_2AlN$ dielectric response investigated by *ab initio* calculations and electron energy-loss spectroscopy

Vincent Mauchamp,[1,*] Gilles Hug,[2] Matthieu Bugnet,[1] Thierry Cabioc'h,[1] and Michel Jaouen[1]
[1]*Laboratoire de Physique des Matériaux (PHYMAT), CNRS, UMR 6630, SP2MI-Boulevard 3, Téléport 2-BP 30179, 86962 Futuroscope Chasseneuil Cedex, France*
[2]*Laboratoire d'Etudes des Microstructures, CNRS-ONERA, Boîte Postale 72, 92322 Châtillon Cedex, France*
(Received 5 October 2009; published 14 January 2010)

This study aims at understanding the anisotropy of the electronic properties of $Ti_2AlN$ at the nanometer scale. The dielectric response of $Ti_2AlN$ single grains was recorded in a transmission electron microscope for the [100] and [001] orientations using high-resolution electron energy-loss spectroscopy. The experimental results are interpreted using *ab initio* calculations based on the density functional theory. The two components of $Ti_2AlN$ dielectric tensor, corresponding to the response within the basal planes of the hexagonal structure and along its *c* axis were computed within the random phase approximation. The results, in good agreement with experiments, show strong anisotropy. Local field effects (LFE), induced by the electronic density inhomogeneities, strongly modify the loss function along the [001] direction, which is dominated by a plasmon, a behavior very similar to the one obtained for pure metals. The dielectric response within the basal plane of the hexagonal structure, more complex, exhibits a plasmonlike behavior together with an interband transition. This interband transition is identified as being characteristic of the N-Ti bonds within the $[Ti_6N]$ octahedra. This study emphasizes the importance of LFE in the response of $Ti_2AlN$ to an electromagnetic perturbation.

DOI: 10.1103/PhysRevB.81.035109 PACS number(s): 79.20.Uv, 71.45.Gm, 71.15.Mb

## I. INTRODUCTION

$Ti_2AlN$ belongs to the wide class of ternary carbides or nitrides called *MAX* phases.[1] These compounds combine the best properties of the ceramics and the metals, which make them very attractive both from the fundamental as well as practical point of view. They follow the composition $M_{n+1}AX_n$, where *M* is an early transition metal, *A* is a group IIIA or IVA element and *X* is either C and/or N. These compounds crystallize in the $P6_3/mmc$ space group (hexagonal Bravais lattice) and their atomic structure can be described as a succession of *n* planes of $[M_6X]$ octahedra separated by layers of atoms *A* (see Fig. 1). Such an anisotropic microstructure has important consequences on the electronic properties of these materials. For instance, it has been shown theoretically that the negligible Seebeck coefficient observed macroscopically for $Ti_3SiC_2$ was due to the combination of a negative thermopower along the *z* axis and a positive one in the basal plane of the hexagonal structure.[2,3] These results were then extended to other *MAX* phases.[4]

The electronic conductivity of these materials is also of great interest since, for instance, $Ti_3SiC_2$ has a better conductivity than elemental titanium. However, the influence of anisotropy on these electronic properties is not yet fully understood. Ground-state density functional theory (DFT) calculations show that electronic carriers at the Fermi level are mostly the transition metal (TM) *d* states what leads some authors to predict a better conductivity along the basal planes than along the **c** axis of the hexagonal structure.[5–7] These results are however only a first approximation since carriers mobility should be considered. Especially, as mentioned by Hug *et al.*, strongly localized *d* states are not expected to have high mobilities.[8] Such results can hardly be confirmed experimentally from usual macroscopic transport properties measurements since these are performed on polycrystalline samples where the contribution from all crystallographic orientations are averaged.[9,10] Recently published results on $Ti_2GeC$ even indirectly show a weak anisotropy by comparing results obtained on a well crystallized thin film to those obtained on bulk polycrystalline samples.[11] Such contradictory observations call for a deeper understanding of the electronic properties of these compounds at the nanometer scale.

The first attempt to have a clear orientation sensitive investigation of the electronic properties of the 211 *MAX* phases was performed recently by Haddad *et al.* on the $Ti_2AlC$ and $Ti_2AlN$ compounds.[12] They used electron energy-loss spectroscopy (EELS) in a transmission electron microscope and focused on the low-loss region (energy-loss $\leq 100$ eV).[13] In this energy range, the EELS scattering cross section is proportional to $\mathrm{Im}\left[\frac{-1}{\varepsilon_M(\mathbf{q},\omega)}\right]$ what gives access to the macroscopic dielectric response of the system, $\varepsilon_M(\mathbf{q},\omega)$, at the nanometer scale. To interpret their spectra, Haddad *et al.* used a phenomenological Drude-Lorentz approach and found that the anisotropy in the $Ti_2AlN$ loss function mainly relies on variations of the plasmon width. This result suggests that the life time of the plasmon oscillation depends on the orientation. However, the EELS signal in this energy range is a mixture between the in-plane and out of plane dielectric responses of the system and such a phenomenological approach does not allow to analyze them separately.

The aim of the present paper is to go beyond the interpretation proposed by Haddad *et al.* and to isolate the two components of $Ti_2AlN$ dielectric tensor corresponding to the in plane, $\varepsilon_{\{\mathbf{a},\mathbf{b}\}}(\mathbf{q},E)$, and out of plane, $\varepsilon_{\{\mathbf{c}\}}(\mathbf{q},E)$, dielectric response using calculations based on the DFT and to relate such calculations to the electronic band structure of the material.[14] $Ti_2AlN$ electronic structure is now well known since it has been widely studied in the literature both experimentally with valence-band photoemission,[15] core-loss spectroscopies,[16] and soft x-ray emission spectroscopy

 

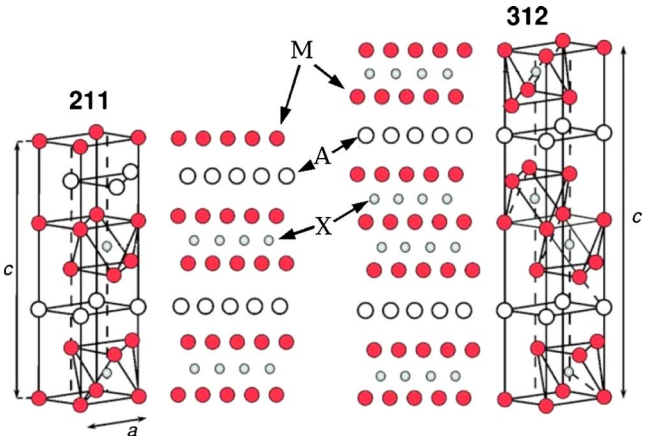


FIG. 1. (Color online) Schematic view of the unit cell of a 211 and 312 *MAX* phase.

experiments,[17] or theoretically with band structure calculations.[7,8,18,19] The bonding scheme in $Ti_2AlN$ is complex, containing a mixed contribution of covalent, metallic and ionic characters. Of special interest for the present study are the Ti *d*-N *p* interactions corresponding to weakly dispersed bands. These "quasi" molecularlike levels of the $[Ti_6N]$ octahedra result from the relocalization of the electron density within these octahedra due to the nitrogen electronegativity.[16] A clear signature of these levels in the loss function will be evidenced.

This paper is organized as follows. The first part is dedicated to the experimental setup, in the second we present the calculation details. In the third part, simulated spectra are compared to experiments. In the last part, the influence of local field effects (LFE) is discussed and the origin of the anisotropic effects in terms of chemical bonding is addressed.

## II. EXPERIMENT

### A. Materials processing

The $Ti_2AlN$ compound has been processed in a bulk polycrystalline state by hot isostatic pressure (HIP) as described by Barsoum *et al.*[20,21] Transmission electron microscope (TEM) samples were cut with a diamond saw, polished and thinned by low-angle (5°) ion milling, using a Gatan PIPS operated at 5 kV. The disturbed layer at the surface was removed with a final polishing step at 2 kV and a very low-angle (2°).

### B. HREELS experiment

High-resolution electron energy-loss spectra (HREELS) were recorded in a ZEISS sesame TEM equipped with a Mandoline energy filter and a monochromated field emission gun. In the energy dispersion plane of the monochromator a 20 $\mu$m slit was inserted. The achieved energy resolution was 0.2 eV as measured from the full-width at half maximum (FWHM) of the elastic peak recorded without a sample. In the back focal plane of the objective lens an aperture limits the integrated signal to a momentum transfer of 0.2 $Å^{-1}$ what corresponds to a collection angle $\beta$ of approximately 0.6 mRad. Under these conditions, the spectra are recorded within the so-called dipolar approximation $[\varepsilon(\mathbf{q},\omega) \simeq \varepsilon(0,\omega)]$ and they can be compared with optical measurements. The raw spectra were corrected from dark noise and gain variations of the detector using the automatic routine provided by the GATAN GIF software. To perform the deconvolution from the multiple losses, the elastic incident energy distribution was recorded separately, without any sample in the path of the swift electrons, in the same experimental conditions. The shape of this peak was adjusted to the experimental spectrum and subtracted from to separate elastic and inelastic events. The spectra were also extrapolated with a so-called "power-function" $I(E)=AE^{-r}$ beyond the energy range of the measured spectrum (in this function $I(E)$ is the measured energy distribution, $E$ is the energy and $A$ and $r$ are fitted parameters). The deconvolution of the spectra was then performed using the standard Fourier-Log procedure to obtain the single scattering loss function $S(\mathbf{q},\omega)$,[13] which is proportional to the inverse of the imaginary part of the macroscopic dielectric function,

$$S(\mathbf{q},\omega) \propto \mathrm{Im}\left(-\frac{1}{\varepsilon_M(\mathbf{q},\omega)}\right). \quad (1)$$

The real and imaginary parts of the dielectric function, $\varepsilon_M(\mathbf{q},\omega)$, are then determined from a Kramers-Kronig analysis (KKA). The output of the KKA gives access to the actual thickness of the specimen. The measurements resulting in a too thin specimen were rejected in order to minimize the surface plasmon contribution. Similarly, the ones originating from too thick specimen were also rejected since the deconvolution process induces a too large noise level. In practice, experiments with specimen thicknesses ranging between 0.3 and 0.7 times the inelastic mean-free path were selected. It should be noted that within this thickness range, no modification of the shape of the deconvolved spectra was observed. We, thus, concluded that the contributions of dynamical diffraction in the spectrum are of minor importance. If present, dynamical effects are of second order compared to the observed anisotropy effects so that they can be neglected in the calculations presented below.

## III. CALCULATION DETAILS

Two codes are used to calculate the dielectric tensor of $Ti_2AlN$: the dielectric properties code (DP) (Ref. 22) which is interfaced with the electronic structure calculation code ABINIT (Ref. 23) and the WIEN2K code and its OPTIC extension.[24,25] The first code is used to investigate the influence of the LFE in both crystallographic orientations. The second approach is used to interpret the structures in the dielectric response in terms of chemical bonding. All calculations were performed in the optic limit, i.e., $\mathbf{q}\rightarrow\mathbf{0}$ ($\mathbf{q}$ being the momentum transfer).

### A. Abinit/DP

The DP code has proved its success in calculating the dielectric tensor of various anisotropic materials.[26,27] It espe-

cially allows the inclusion of LFE and to go beyond the random phase approximation (RPA), namely, including exchange and correlation effects in the response function.[28,29] In the present study, we will stay at the RPA level and will only be concerned by the LFE and their strongly anisotropic behavior.

The LFE arise in inhomogeneous periodic crystals from the microscopic fields induced by an electromagnetic perturbation. These fields vary rapidly with respect to the unit cell size and appear in the $\mathbf{G} \neq \mathbf{0}$ Fourier components of the calculated total field in the material ($\mathbf{G}$ being a reciprocal-lattice vector). These microscopic components are expressed in terms of nondiagonal elements in the calculated Fourier transformed microscopic dielectric matrix $\varepsilon_{\mathbf{GG}'}(\mathbf{q},\omega)$. EELS experiments probing the imaginary part of the inverse of the macroscopic dielectric tensor $\varepsilon_M(\mathbf{q},\omega)$, one thus has to take the average of the microscopic dielectric matrix over the unit cell to simulate the experimental spectra, which in Fourier space can be written as[30,31]

$$\varepsilon_M(\mathbf{q},\omega) = \frac{1}{[\varepsilon^{-1}_{\mathbf{GG}'}(\mathbf{q},\omega)]_{\mathbf{G}=\mathbf{G}'=0}}, \tag{2}$$

where $[\varepsilon^{-1}_{\mathbf{GG}'}(\mathbf{q},\omega)]_{\mathbf{G}=\mathbf{G}'=0}$ is the $\mathbf{G}=\mathbf{G}'=\mathbf{0}$ term of the inverse of $\varepsilon_{\mathbf{GG}'}(\mathbf{q},\omega)$.

In the DP code, the inverse of $\varepsilon_{\mathbf{GG}'}(\mathbf{q},\omega)$ is obtained from the linear-response polarizability $\chi_{\mathbf{GG}'}(\mathbf{q},\omega)$ according to the following matrix equation:

$$\varepsilon^{-1}_{\mathbf{GG}'}(\mathbf{q},\omega) = \delta_{\mathbf{GG}'} + V_C(\mathbf{q}+\mathbf{G})\chi_{\mathbf{GG}'}(\mathbf{q},\omega), \tag{3}$$

where $V_C(\mathbf{q}+\mathbf{G})$ is the bare coulomb potential. Within the RPA, $\chi_{\mathbf{GG}'}(\mathbf{q},\omega)$ is deduced from the independent particle polarizability $\chi^{(0)}_{\mathbf{GG}'}(\mathbf{q},\omega)$ according to:

$$\chi_{\mathbf{GG}'} = [\delta_{\mathbf{GG}'} - \chi^{(0)}_{\mathbf{GG}'}V_C(\mathbf{q}+\mathbf{G})]\chi^{(0)}_{\mathbf{GG}'}. \tag{4}$$

The independent polarizability $\chi^{(0)}_{\mathbf{GG}'}(\mathbf{q},\omega)$, expressed in terms of independent transitions between the single particle states $|\Psi\rangle$ of the systems, is given by:[30,31]

$$\chi^{(0)}_{\mathbf{GG}'} = 2\sum_{i,f}(f_f - f_i)\frac{\langle\Psi_i|e^{-i(\mathbf{q}+\mathbf{G}).\mathbf{r}}|\Psi_f\rangle\langle\Psi_f|e^{i(\mathbf{q}+\mathbf{G}').\mathbf{r}}|\Psi_i\rangle}{\varepsilon_f - \varepsilon_i - \hbar\omega - i\eta}, \tag{5}$$

where $f_i$ and $f_f$ are the occupation numbers, and $\varepsilon_i$ and $\varepsilon_f$ are the eigenenergies of the initial and final single particle states $|\Psi_i\rangle$ and $|\Psi_f\rangle$, respectively. In these expressions, the indexes $i$ and $f$ refer to the band index $n$ and the crystal momentum $\boldsymbol{k}$. The calculated macroscopic dielectric tensor including LFE can thus be deduced from the Kohn-Sham (KS) orbitals obtained from DFT calculations. Although rigorously not an excited state theory, the DFT has been shown to give very good results for such calculations.

The electronic structure calculations were performed with the pseudopotential code Abinit within the generalized gradient approximation (GGA).[23,32] Troullier Martins norm-conserving pseudopotentials from the Abinit database were used for the aluminum and nitrogen atoms.[33] Concerning the titanium atom, semicore states (the titanium $3s$ and $3p$ states) were considered in the pseudopotential which was taken from the OPIUM code database.[34] Due to the presence of the semicore states, the titanium pseudopotential is quite "hard" and a plane-wave cutoff of 46 Ry was necessary to achieve full convergence of the total energy. The accuracy of the pseudopotentials was checked by comparing the optimized unit cell parameters obtained with Abinit to those obtained from the all electron calculations of Hug *et al.*[16] Results are in very good agreement (they differ by less than 1%). This is confirmed by the calculations of the total density of states (DOS), which give identical results to those obtained from WIEN2K (not shown here). We are, thus, confident that the pseudopotentials used in the calculation are reasonably accurate. This is clear when comparing the imaginary part of $\varepsilon_{\{\mathbf{c}\}}(\mathbf{0},E)$ ignoring LFE calculated with DP in Fig. 5 to that obtained from WIEN2K in Fig. 7, both being very similar.

TABLE I. Main parameters used for the Abinit/DP (top) and WIEN2K/OPTIC (down) calculations. The numbers in the k-point columns refer to the sampling of the irreducible part of the Brillouin zone.

| Abinit | | DP | |
|---|---|---|---|
| $E_{cut}$ (Ha) | $k$ points (SCF) | $k$ points | **G** vectors |
| 46 | 128 | 98 | Ti $M_{2,3}$ edge: 177<br>Plasmon [100]: 107<br>Plasmon [001]: 55 |
| WIEN2K | | OPTIC | |
| $RK_{max}$ | $k$ points (SCF) | $k$ points | |
| 7.5 | 80 | 195 | |

Convergence on the matrix size for the calculation of $\chi^{(0)}_{\mathbf{GG}'}(\mathbf{q},\omega)$ was different depending on the considered signature in the EELS spectrum. Focusing on the plasmon region (below 30 eV), 107 **G** vectors had to be considered for the [100] direction and only 55 for the [001] direction. For the titanium $M_{2,3}$ edge (around 45 eV), 177 **G** vectors were considered in both crystallographic orientations. All calculation details are given in Table I.

### B. WIEN2k

WIEN2k calculations are based on a full potential band-structure approach: valence or conduction KS wave functions are described as Bloch states. Wave functions, as well as potentials, are described in the whole space using a muffin-tin (MT) approach consisting of nonoverlapping spheres centered at each atomic site. No approximation is made on the shape of the potentials in the interstitial region. Inside the MT spheres, the KS wave functions are developed on a linearized augmented plane wave (LAPW) basis set or an augmented plane wave (APW) basis set combined with local orbitals (lo), (APW+lo).[35,36] This second approach was used in the present paper. Plane waves are used in the interstitial space. Core electrons are explicitly treated with a relativistic atomic code:[37,38] WIEN2K is, thus, an all electron code

which makes a big difference with respect to Abinit. The LAPW treatment as implemented in WIEN2K is one of the most accurate method for electronic structure calculations. For comparison with the Abinit/DP results, calculations were performed considering the same GGA exchange and correlation potential.[32] All calculation details are given in Table I.

Dielectric tensor calculations can be performed from the calculated electronic structure thanks to the OPTIC package:[25] one can access to the RPA dielectric tensor ignoring the LFE. The calculated dielectric function is given in terms of independent inter(intra)-band transitions so that the WIEN2K calculations will be used to clearly identify the transitions responsible for the principal structures observed on the experimental spectra.

Abinit/DP and WIEN2k calculations are very complementary. The first one is used to compute as accurately as possible the macroscopic dielectric tensor of $Ti_2AlN$ while the second one allows the precise interpretation of its dielectric response in terms of chemical bonding.

## IV. RESULTS: COMPARISON EXPERIMENT/THEORY

Due to the finite collection angle $\beta$ of the microscope, the EELS signal in the low-loss region is always a mix between the dielectric response parallel to the electron beam $\varepsilon_{\parallel}$ and the one in the perpendicular direction $\varepsilon_{\perp}$. For comparison with the experiment, we thus used the expression given by Vast *et al.*, which gives the EELS intensity integrated over the collection angle as a function of the dielectric response perpendicular and parallel to the electron beam,[39]

$$I(E) \propto -\mathrm{Im}\left\{\frac{\pi}{\varepsilon_{\perp}(0,E)}\ln\left[1+\frac{\beta^2\varepsilon_{\perp}(0,E)}{\theta_E^2\varepsilon_{\parallel}(0,E)}\right]\right\}, \qquad (6)$$

where $\beta$ is the collection angle and $\theta_E$ is the characteristic angle at energy-loss $E$ ($\theta_E=E/(\gamma m_0 v^2)=0.046$ mrad).[13] In the [001] zone axis, $\varepsilon_{\perp}(0,E)$ and $\varepsilon_{\parallel}(0,E)$ correspond respectively to $\varepsilon_{\{\mathbf{a},\mathbf{b}\}}(0,E)$ and $\varepsilon_{\{\mathbf{c}\}}(0,E)$. In the [100] zone axis, we took $\varepsilon_{\perp}(0,E)$ as the average of $\varepsilon_{\{\mathbf{a},\mathbf{b}\}}(0,E)$ and $\varepsilon_{\{\mathbf{c}\}}(0,E)$. Comparison between the experimental and theoretical spectra is given in Fig. 2. Best fits were obtained for $\beta=0.6$ and 0.28 mrad for the [100] and [001] orientations, respectively. These values are in good agreement with the experimental one ($\beta_{\mathrm{exp}}\sim 0.6$ mrad, see Sec. II B) and support the validity of Eq. (6). The slight difference between the $\beta$ obtained in the two orientations can be due to either a little change in the experimental conditions when tilting the sample or to the different dispersion behavior of the dielectric function. Indeed, Eq. (6) is only approximate since the **q** dependence of the dielectric function is ignored: such effects are left to further studies. Finally, for comparison with the experiments, a 1.5 eV Lorentzian broadening was applied to the theoretical spectra.

When focusing on Fig. 2, one can see that the two major structures A and B are well reproduced in terms of energy and relative intensities. However, several discrepancies can be observed: the plasmon width variation when tilting from the [100] to [001] orientations is not well reproduced. This is probably due to the fact that the **q** dispersion of the dielectric function is ignored in the present calculations. Although the relative intensities between the titanium $M_{2,3}$ edge and structures A and B is well reproduced, its theoretical energy is too small compared to the experiment. The maximum of the titanium $M_{2,3}$ edges is calculated around 43.8 eV whereas the experimental ones is 47.6 eV. Self-energy effects should be included to correct from such an energy shift and one needs to go beyond the one electron approximation.[40] The overall agreement is however quite good. Except the variations of the plasmon width, the anisotropic effects observed experimentally are rather small because of the unavoidable mix between the in plane and out of plane dielectric responses.

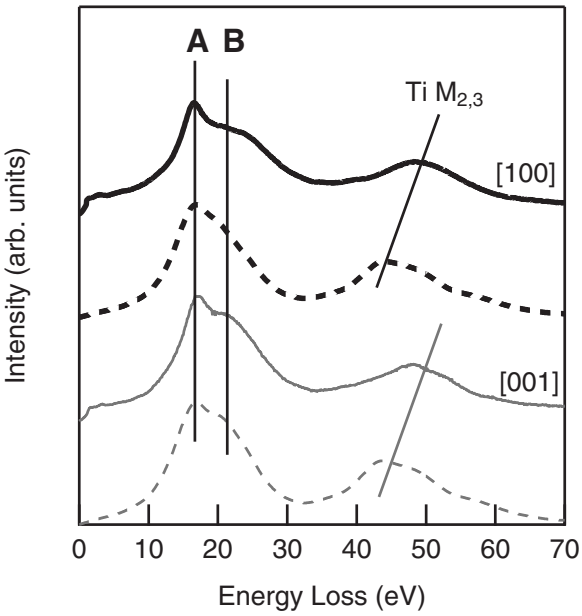


FIG. 2. Comparison between the HREELS spectra (full lines) and DP simulations (dashed lines) recorded along the [100] (black) and [001] (gray) zone axis. Calculations were performed including LFE.

To get more insight in the anisotropy of the dielectric response of $Ti_2AlN$, the pure longitudinal loss function, and the associated real and imaginary parts of $\varepsilon_M(\mathbf{0},\omega)$ calculated within the basal plane or along the **c** axis, are shown in Fig. 3. These theoretical spectra would be those obtained from EELS experiments for a zero collection angle, and the corresponding imaginary part of $\varepsilon_M(\mathbf{0},\omega)$ from linearly polarized optic experiments. It is clear from Fig. 3(a) that the loss function within the basal plane is different from the one along the **c** axis. In the first case, the two structures A and B clearly appear with very similar intensities whereas the loss function obtained perpendicularly to the basal plane is dominated by structure A, structure B being totally absent from the spectrum. Focusing now on the real and imaginary parts of $\varepsilon_{\{\mathbf{a},\mathbf{b}\}}(\mathbf{0},E)$ and $\varepsilon_{\{\mathbf{c}\}}(\mathbf{0},E)$ given in Figs. 3(b) and 3(c), respectively, one can see that structures A and B are totally different in nature. In both components of the dielectric response, the structure A corresponds to a zero of the real part of the dielectric function and to no particular structure in the imaginary part. This is characteristic of a plasmon, a longitudinal collective mode.[41] On the other hand, structure B, which is missing in the loss function related to the [001]

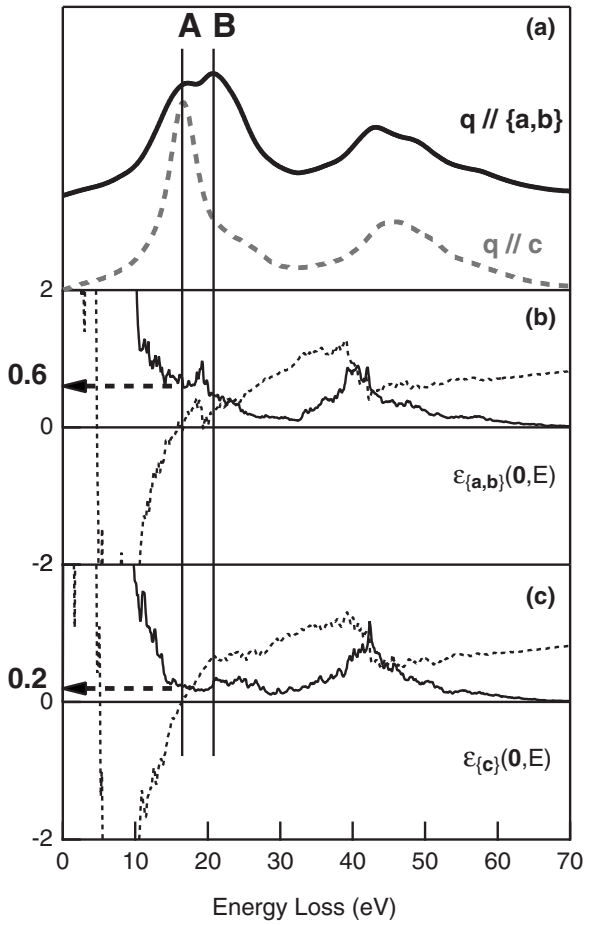


FIG. 3. (a) Loss functions calculated using $\varepsilon_{\{\mathbf{a},\mathbf{b}\}}(\mathbf{0},E)$ (black lines) or $\varepsilon_{\{\mathbf{c}\}}(\mathbf{0},E)$ (gray lines). The real (dots) and imaginary (full lines) parts of $\varepsilon_{\{\mathbf{a},\mathbf{b}\}}(\mathbf{0},E)$ and $\varepsilon_{\{\mathbf{c}\}}(\mathbf{0},E)$ are given in (b) and (c), respectively. Calculations were performed with DP including the LFE. In (b) and (c), a 0.1 eV lorentzian broadening was applied.

response, is due to an absorption peak in $\mathrm{Im}[\varepsilon_{\{\mathbf{a},\mathbf{b}\}}(\mathbf{0},E)]$ associated to an oscillation in the real part. This is characteristic of an interband transition. The energy shift observed between the absorption peak in $\mathrm{Im}[\varepsilon_{\{\mathbf{a},\mathbf{b}\}}(\mathbf{0},E)]$ and peak B is a well known effect of the calculation of the loss function.[42]

Thus, although the anisotropy observed in the EELS spectra given in Fig. 2 is small, the response functions obtained from each components of the dielectric tensor reveal a strong anisotropy in the dielectric behavior of $Ti_2AlN$ in the UV energy range. Within the basal planes, the dielectric behavior is a complex mix between an interband transition and a plasmon. Along the **c** axis, the dielectric response is dominated by a plasmon: the dielectric behavior is here close to the one observed for a simple metal.[41]

## V. DISCUSSION

### A. Influence of local field effects

To obtain the results above reported, LFE had to be included. These microscopic depolarizating fields are the major cause for the observed anisotropy in the dielectric response. This is illustrated in Fig. 4 where are plotted the in-plane and

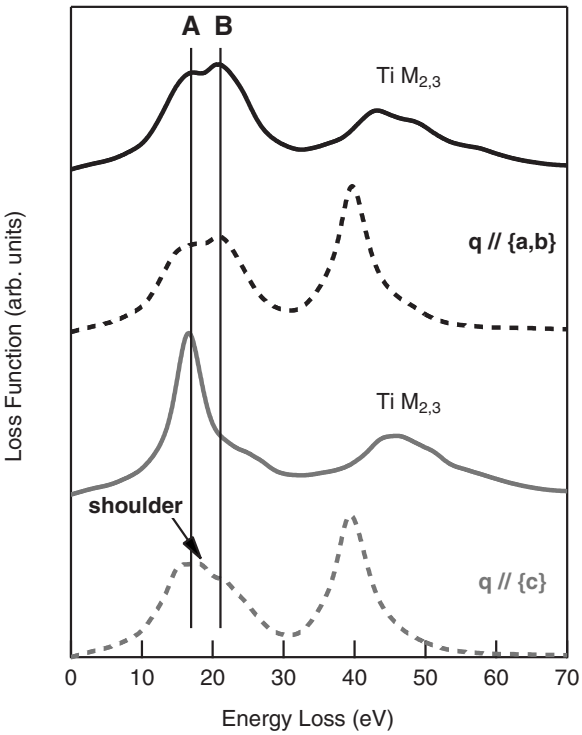


FIG. 4. Loss functions calculated from $\varepsilon_{\{\mathbf{a},\mathbf{b}\}}(\mathbf{0},E)$ (black) and $\varepsilon_{\{\mathbf{c}\}}(\mathbf{0},E)$ (gray) with (full lines) or without (dashed lines) the LFE. Calculations were performed with DP.

out-of-plane loss functions calculated considering or not the LFE.

Focusing first on the high energy part of the EELS spectra, one can see that the LFE at the titanium $M_{2,3}$ edges are very important as already observed in the case of $TiO_2$.[39] For both orientations, the LFE strongly decrease the intensity of the edges and shift them to higher energies, improving the agreement with the experiments. As demonstrated by Aryasetiawan *et al.* for nickel and nickel oxide, the LFE are directly related to the magnitude of a Coulomb integral for a charge density $\rho_\mu(\mathbf{r})-\rho_{av}$.[43] In a simple two band model $\rho_\mu(\mathbf{r})$ is the product of the two wave functions involved in the transition (here the titanium $3p$ and $3d$ states) and $\rho_{av}$ is the average of this product. For transition metals $M_{2,3}$ edges, $\rho_\mu(\mathbf{r})-\rho_{av}$ is quite large and it leads to important LFE. Due the atomic origin of these LFE, they are not sensitive to the anisotropy of the crystal structure (they have equal magnitude in the [100] and [001] orientation) and a high number of **G** vectors must be included to describe such an atomic scale process (177 **G** in the present case) when calculating $\chi^{(0)}_{\mathbf{G}\mathbf{G}'}(\mathbf{0},\omega)$.

Focusing now on the low-energy range of the spectra (below 30 eV), the LFE have different magnitude when calculated within the $\{\mathbf{a},\mathbf{b}\}$ plane or along the **c** axis. In the first case, it is clear that LFE have little influence on the two structures A and B leading to a complex dielectric response (a mixture of a plasmon and interband transitions). Along the **c** axis, the LFE have a much more pronounced influence: they strongly reduce the interband transition B as well as the shoulder (arrowed in the figure) observed after the plasmon A, which is slightly shifted toward higher energies. This can

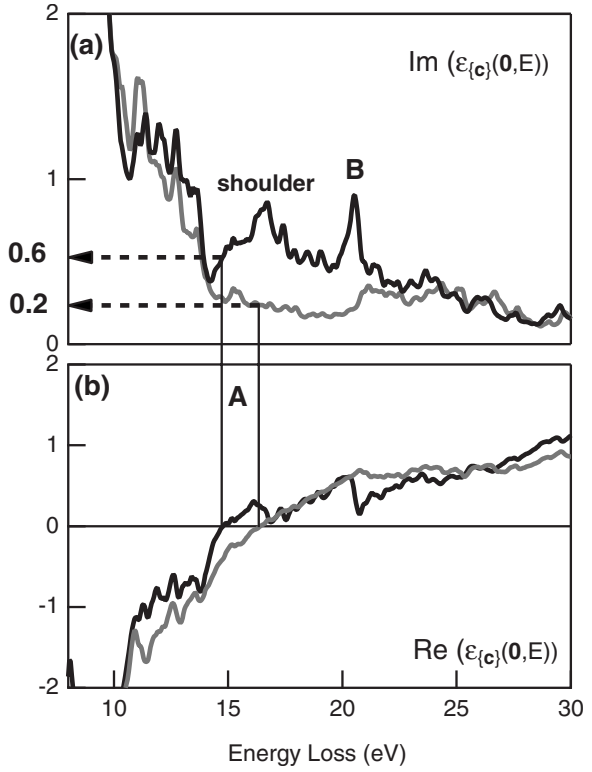


FIG. 5. Imaginary (a) and real (b) parts of $\varepsilon_{\{\mathbf{c}\}}(\mathbf{0},E)$ calculated with (gray lines) or without (black lines) the LFE. Calculations were performed with DP. A 0.1 eV lorentzian broadening was applied.

be clearly seen in Fig. 5 where are plotted the real and imaginary parts of $\varepsilon_{\{\mathbf{c}\}}(\mathbf{0},E)$ calculated with or without the LFE. The structures corresponding to the shoulder and peak B in the loss function disappear when LFE are included. The direct consequence is that the loss function is dominated by the plasmon in this orientation even if a remaining small bump is still visible on the right side of the plasmon in Fig. 4.

Following the nearly free electron model described by Sturm,[41] to observe, at the plasmon energy $E_p$ obtained from $\mathrm{Re}\{\varepsilon_M(\mathbf{0},E_p)\}=0$, a nonzero imaginary part of $\varepsilon_M(\mathbf{0},E_p)$ implies that the plasmon can promote interband transitions at $E_p$. Within this simple model (i.e., only taking electronic effects into account) the plasmon width at half maximum is proportional to $\mathrm{Im}[\varepsilon_M(\mathbf{0},E_p)]$. Thus, as can be seen from Fig. 5, the plasmon linewidth along the **c** axis of the $Ti_2AlN$ structure is reduced by roughly a factor of three when LFE are taken into account: $\mathrm{Im}[\varepsilon_{\{\mathbf{c}\}}(\mathbf{0},E_p)]$ decreases from 0.6 to 0.2. Comparing Figs. 3(b) and 3(c) and following the same line of reasoning, one can see that the plasmon linewidth within the basal plane of the hexagonal structure is three times larger than along the **c** axis. According to the free electron model this implies that the plasmon lifetime is three times larger in the [001] orientation than within the basal planes. However, such a plasmon decay mechanism will provide only an underestimate for its lifetime because phonons and defects are ignored. They should of course be taken into account to provide a complete description for plasmons decay mechanism.

If LFE are ignored, the difference between the two orientations is reduced (dashed curves in Fig. 4): the two structures A and B are observed to exist for both orientations and the main difference relies in the variation of their relative intensities. This emphasizes that the anisotropy in the dielectric response of $Ti_2AlN$ is mainly driven by LFE. These LFE are different in nature from those observed at the titanium $M_{2,3}$ edges since they involve much more delocalized wave functions. They are linked to the strong inhomogeneity of the electron density along the **c** axis due to the alternance of aluminum and $[Ti_6N]$ octahedra layers with a strong localization of the electron density within this octahedra.[16] The corresponding induced fields have thus long wavelength with respect to those observed at the Ti $M_{2,3}$ edges and LFE are converged using only 55 **G** vectors in $\chi^{(0)}_{\mathbf{GG}'}(\mathbf{0},\omega)$. Such a structural anisotropy of the LFE was already observed in layered compounds such as graphite or boron nitride.[44]

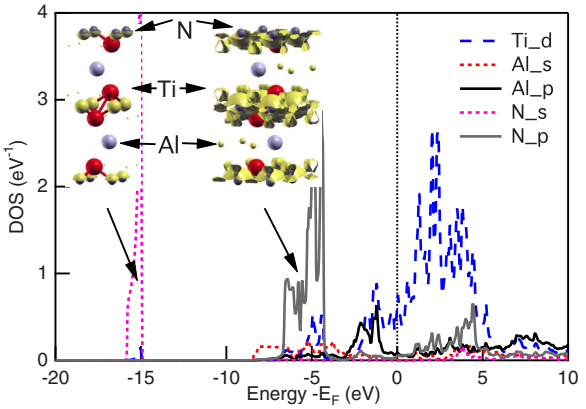


FIG. 6. (Color online) WIEN2k $Ti_2AlN$ density of states (DOS) projected on the Ti *d* (dashed blue lines), Al *s* (red dots), Al *p* (black lines), N *s* (pink dots), and N *p* states (gray line). The multiplicity of atoms is not taken into account. The electron densities corresponding the N *s* states and the N *p*-Ti *d* hybridization are plotted.

### B. Origin of the interband transitions

To understand the origin of the interband transitions responsible for the shoulder and peak B observed in the loss functions calculated without LFE, the components of the dielectric tensor have been calculated from the independent particle polarizability using WIEN2K and its LAPW approach. Using the OPTIC program, the imaginary part of the dielectric function can be computed restricting the summation to selected band indexes involved in the Eq. (5). It is then possible to investigate the influence of the bonding scheme on the dielectric properties. As shown in Fig. 6, the valence band of $Ti_2AlN$ can be schematically divided into three regions (we only focus on the energy range above −20 eV below the Fermi energy). The first one, between −16 and −15 eV, corresponds essentially to the weakly dispersed nitrogen *s* bands. Between −8.5 and −4 eV are bands characteristic of the hybridization between Ti *d* and N *p* states giving rise to bonding interactions as demonstrated by the balanced crystal overlap population calculations performed by Magnuson *et al.*[17] Finally, between −3 and −0.8 eV are the levels characteristic of the bonding interactions between

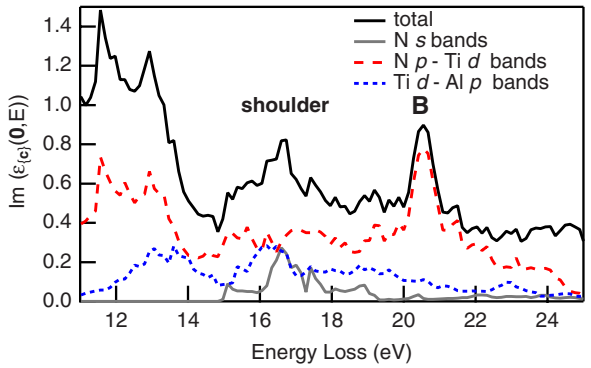


FIG. 7. (Color online) Imaginary part of $\varepsilon_{\{\mathbf{c}\}}(\mathbf{0},E)$ calculated considering separately the bands corresponding to the N *s* states (gray line), the N(*p*)-Ti(*d*) interactions (dashed lines) and the Ti(*d*)-Al(*p*) interactions (dots). For comparison the result obtained considering all the transitions is also given (black line). Calculations were performed with WIEN2K.

the Ti *d* and Al *p* states. The electron densities corresponding the two first groups of bands are also plotted in Fig. 6: these plots illustrate the strong inhomogeneity of the electron density responsible for the LFE observed in $\varepsilon_{\{\mathbf{c}\}}(\mathbf{0},E)$.

To analyze the origins of the absorption peaks observed between 10 and 30 eV in the loss function calculated from $\mathrm{Im}[\varepsilon_{\{\mathbf{c}\}}(\mathbf{0},E)]$, the contribution of each of these groups of bands have been computed separately. The obtained $\mathrm{Im}[\varepsilon_{\{\mathbf{c}\}}(\mathbf{0},E)]$ are plotted in Fig. 7. The result obtained when considering all bands in the calculation is also given for comparison. It is clear from Fig. 7 that, in the region of interest between 14 and 24 eV, all three groups of bands above mentioned contribute to the dielectric function. Peak B is mainly due to excitations of the weakly dispersed bonding states resulting from the N *p*-Ti *d* interactions. This structure is characteristic of the $[Ti_6N]$ octahedra layers. Considering the structure appearing as a shoulder in the loss function obtained from the independent particle polarizability, it is a mix between excitations from the N *s* bands and the bonding states resulting from the hybridization between the Ti *d* and Al *p* states. Although different in nature, these two structures, that vanish for the [001] orientation when local fields are included, are in part or fully due to excitations of states corresponding to the $[Ti_6N]$ octahedra layers. The $[Ti_6N]$ octahedra being highly polarizable entities (see the important charge transfers calculated on the *X* atoms by Hug *et al.* in these 211 phases)[16] the induced fields are important and almost compensate the external perturbation. This leads to a strong reduction of the excitations of the corresponding structures. Considering the dielectric response within the $\{\mathbf{a},\mathbf{b}\}$ plane, the electronic density inhomogeneity is much weaker so that LFE are less important and structure B is observed in the calculated loss function either considering LFE or not.

## VI. CONCLUSION

The anisotropy of the dielectric response of $Ti_2AlN$ single grains has been studied combining high-resolution electron energy-loss spectroscopy and *ab initio* calculations based on the density functional theory. Dielectric function calculations were performed within the random phase approximation and local field effects had to be included to reproduce the experimental spectra. Due to the experimental setting, when the swift electrons travel perpendicular to the sixfold axis, the recorded spectrum is an average of the dielectric response parallel and perpendicular to the **c** axis. Thus, only a reduced anisotropy is observed when tilting from the [100] to the [001] zone axis. This is confirmed by the theoretical results obtained by integrating the two components of the dielectric tensor corresponding to the dielectric response within the basal planes of the hexagonal structure, $\varepsilon_{\{\mathbf{a},\mathbf{b}\}}(\mathbf{0},E)$, and parallel to the **c** axis, $\varepsilon_{\{\mathbf{c}\}}(\mathbf{0},E)$.

Analyzed separately, the loss functions deduced from $\varepsilon_{\{\mathbf{a},\mathbf{b}\}}(\mathbf{0},E)$ and $\varepsilon_{\{\mathbf{c}\}}(\mathbf{0},E)$ however show very different behaviors, emphasizing the important anisotropy of $Ti_2AlN$ dielectric response. Within the basal planes, the dielectric response in the UV energy range, as probed by EELS, is a complex mix between a plasmon and an interband transition. This interband transition has been identified as being characteristic of the $[Ti_6N]$ octahedra layers. Along the **c** axis, the loss function is dominated by a plasmon, a behavior very close to that observed in simple metals. Such an anisotropy is mainly due to the local field effects that arise from inhomogeneities of $Ti_2AlN$ electronic density. These LFE, particularly important along the **c** axis, strongly reduce the interband transitions around the plasmon energy. The plasmon lifetime is thus enhanced in the [001] direction since possible decay in terms of single particle excitations are reduced. All the here presented results were obtained within the optic limit $(\mathbf{q}\rightarrow 0)$ and the dispersion of the dielectric function should also be considered. Such a study is in progress.

The results presented here show that the interactions between *MAX* phases and an electromagnetic field cannot be simply treated in terms of independent particle transitions. More complex phenomena have to be considered to properly reproduce the physics behind.

*vincent.mauchamp@univ-poitiers.fr

[1] M. W. Barsoum, Prog. Solid State Chem. **28**, 201 (2000).
[2] H.-Y. Yoo, M. W. Barsoum, and T. El-Raghy, Nature (London) **407**, 581 (2000).
[3] L. Chaput, G. Hug, P. Pécheur, and H. Scherrer, Phys. Rev. B **71**, 121104(R) (2005).
[4] L. Chaput, G. Hug, P. Pécheur, and H. Scherrer, Phys. Rev. B **75**, 035107 (2007).
[5] Z. Sun and Y. Zhou, Phys. Rev. B **60**, 1441 (1999).
[6] Y. Zhou and Z. Sun, Phys. Rev. B **61**, 12570 (2000).
[7] Y. C. Zhou, H. Y. Dong, X. H. Wang, and S. Q. Chen, J. Phys.: Condens. Matter **12**, 9617 (2000).

[8] G. Hug and E. Fries, Phys. Rev. B **65**, 113104 (2002).
[9] M. W. Barsoum, H.-I. Yoo, I. K. Polushina, V. Yu. Rud', Yu. V. Rud', and T. El-Raghy, Phys. Rev. B **62**, 10194 (2000).
[10] J. D. Hettinger, S. E. Lofland, P. Finkel, T. Meehan, J. Palma, K. Harrell, S. Gupta, A. Ganguly, T. El-Raghy, and M. W. Barsoum, Phys. Rev. B **72**, 115120 (2005).
[11] T. H. Scabarozi, P. Eklund, J. Emmerlich, H. Högberg, T. Meehan, P. Finkel, M. W. Barsoum, J. D. Hettinger, L. Hultman, and S. E. Lofland, Solid State Commun. **146**, 498 (2008).
[12] N. Haddad, E. Garcia-Caurel, L. Hultman, M. W. Barsoum, and G. Hug, J. Appl. Phys. **104**, 023531 (2008).
[13] R. Egerton, *Electron Energy-Loss Spectroscopy in the Electron Microscope* (Plenum, New York, 1996).
[14] R. O. Jones and O. Gunnarsson, Rev. Mod. Phys. **61**, 689 (1989).
[15] L. Soriano, M. Abbate, H. Pen, P. Prieto, and J. M. Sanz, Solid State Commun. **102**, 291 (1997).
[16] G. Hug, M. Jaouen, and M. W. Barsoum, Phys. Rev. B **71**, 024105 (2005).
[17] M. Magnuson, M. Mattesini, S. Li, C. Höglund, M. Beckers, L. Hultman, and O. Eriksson, Phys. Rev. B **76**, 195127 (2007).
[18] B. Holm, R. Ahuja, S. Li, and B. Johansson, J. Appl. Phys. **91**, 9874 (2002).
[19] Z. Sun, D. Music, R. Ahuja, and J. M. Schneider, Phys. Rev. B **71**, 193402 (2005).
[20] M. W. Barsoum, D. Brodkin, and T. El-Raghy, Scr. Mater. **36**, 535 (1997).
[21] M. W. Barsoum and T. El-Raghy, J. Am. Ceram. Soc. **79**, 1953 (1996).
[22] V. Olevano, L. Reining, and F. Sottile, http:\\www.dp-code.org.
[23] X. Gonze, J.-C. Beuken, R. Caracas, F. Detraux, M. Fuchs, G.-M. Rignanese, L. Sindic, M. Verstraete, G. Zerah, F. Jollet, M. Torrent, A. Roy, M. Mikami, P. Ghosez, J.-Y. Raty, and D. C. Allan, Comput. Mater. Sci. **25**, 478 (2002).
[24] P. Blaha, K. Schwarz, G. K. H. Madsen, D. Kvaniscka, and J. Luitz, *WIEN2k, An Augmented Plane Wave+Local Orbitals Program for Calculating Crystal Properties* (Technische Universität Wien, Austria, 2001).
[25] C. Ambrosch-Draxl and J. O. Sofo, Comput. Phys. Commun. **175**, 1 (2006).
[26] A. G. Marinopoulos, L. Reining, V. Olevano, A. Rubio, T. Pichler, X. Liu, M. Knupfer, and J. Fink, Phys. Rev. Lett. **89**, 076402 (2002).
[27] A. G. Marinopoulos, L. Reining, A. Rubio, and N. Vast, Phys. Rev. Lett. **91**, 046402 (2003).
[28] L. Reining, V. Olevano, A. Rubio, and G. Onida, Phys. Rev. Lett. **88**, 066404 (2002).
[29] F. Sottile, V. Olevano, and L. Reining, Phys. Rev. Lett. **91**, 056402 (2003).
[30] N. Wiser, Phys. Rev. **129**, 62 (1963).
[31] S. L. Adler, Phys. Rev. **126**, 413 (1962).
[32] J. P. Perdew, K. Burke, and M. Ernzerhof, Phys. Rev. Lett. **77**, 3865 (1996).
[33] N. Troullier and J. L. Martins, Phys. Rev. B **43**, 1993 (1991).
[34] http:\\opium.sourceforge.net.
[35] G. K. H. Madsen, P. Blaha, K. Schwarz, E. Sjöstedt, and L. Nordström, Phys. Rev. B **64**, 195134 (2001).
[36] E. Sjöstedt, L. Nordström, and D. J. Singh, Solid State Commun. **114**, 15 (2000).
[37] J. Desclaux, Comput. Phys. Commun. **1**, 216 (1970).
[38] J. Desclaux, Comput. Phys. Commun. **9**, 31 (1975).
[39] N. Vast, L. Reining, V. Olevano, P. Schattschneider, and B. Jouffrey, Phys. Rev. Lett. **88**, 037601 (2002).
[40] L. Hedin, Phys. Rev. **139**, A796 (1965).
[41] K. Sturm, Adv. Phys. **31**, 1 (1982).
[42] V. J. Keast, J. Electron Spectrosc. Relat. Phenom. **143**, 97 (2005).
[43] F. Aryasetiawan, O. Gunnarsson, M. Knupfer, and J. Fink, Phys. Rev. B **50**, 7311 (1994).
[44] A. G. Marinopoulos, L. Wirtz, A. Marini, V. Olevano, A. Rubio, and L. Reining, App. Phys. A **78**, 1157 (2004).